Transition Dipole Moments of One-Dimensional Excitons in Soluble Phthalocyanine Thin Films

Libin Liang[†], KimNgan Burrill[†,‖], and Madalina I. Furis*[,†,§]

[†]Materials Science Program and Department of Physics, University of Vermont, 82 University Place, Burlington, Vermont 05405, United States

[‖]Intel Corporation, Rio Rancho, NM 87124, United States

[§]Homer L. Dodge Physics Department, University of Oklahoma, Norman, OK 73019, United States

*Email: madalina.furis@ou.edu. Tel.: (405) 934 2221

Abstract

We report on polarization-resolved absorption and photoluminescence spectroscopy experiments that investigate the spatial orientation of excitonic transition dipoles at temperature ranging from 4 K to room temperature, in crystalline phthalocyanine thin films prepared with solution-based deposition methods. Octabutoxy phthalocyanines are quasi 1D systems, with highly directional intermolecular interactions along a preferred crystalline axis. Experiments reveal the existence of red-shifted delocalized, bulk bandgap exciton states at temperatures below 175 K. These states are the result of the strong π-π short-range coupling and long-range Coulomb coupling between nearest neighbour molecules along the stacking axis. They are characterized by linearly polarized, non-degenerate dipoles that largely obey the Davydov selection rules. The photoluminescence studies reveal these excitons couple to lattice and molecular vibrations, forming delocalized exciton-polarons at temperature below 175 K. Finally, by changing the incident light wavevector orientation we find additional, circularly and elliptical polarized states that most likely result from the mixing of HOMO-n (n >1) orbitals with aza nitrogen orbitals.

Introduction

Organic molecules, such as pentacene, rubrene and phthalocyanine which have well-defined π-conjugated systems and exhibit great charge carrier mobility, are at the frontier of electronic materials research and represent the feasible alternative to traditional silicon-based semiconductor applications like field-effect transistors (OFETs) and photovoltaic devices (OPVs) when flexible electronics platforms are required[1-5]. Molecular systems with large intermolecular interactions easily self-assemble into crystalline thin films, a highly desirable characteristic for organic semiconductors[6-8]. Large enhancements in charge carrier mobility

and exciton diffusion length are routinely reported when amorphous thin films in devices are replaced with polycrystallline thin films or single crystals[7, 9-14]. Most notably, the formation of robust coherent excitonic states in the low dimensional small molecule semiconductors[15-16] opens the possibility of ballistic exciton diffusion[12-14, 17-20], fast carrier transport[21] and formation of topologically protected states[22]. In this context, knowledge of the excitonic states symmetries in the solid state is crucial, since the topological applications require orbitally -degenerate states[22].

Phthalocyanine (Pc) and its derivatives are widely utilized in different applications because of their easy synthesis, high stability and tunable π-π* transition in the visible/near IR region[23-24]. Octabutoxy phthalocyanine (H_2-OBPc) is a soluble derivative of the Pc which has eight butoxy electron-donating group at the non-peripheral benzo positions. It features highly directional intermolecular interactions in the crystalline phase due to the nearest -neighbor π-orbital overlap and thus has self-assembly properties which lead to long-range molecular ordering[25] and a one-dimensional character for carrier or exciton transport[16, 26]. Previous experiments report that H_2-OBPc crystalline thin films with grain sizes on millimeter-scale are obtained with solution-based deposition methods[26-28]. These ordered thin films with large grain sizes uniquely offer the opportunity to spatially explore optical and excitonic properties within a single crystalline grain, free from the influence of grain boundaries or static disorder, enabling the usage of a variety of diffraction-limited optical techniques at low temperatures in a variety of experimental geometries. Theoretical studies[16, 29] indicate that crystalline phthalocyanines are characterized by strong short range intermolecular exchange interactions , comparable to the reorganization energy for exciton energy transfer. In such systems, the dynamic disorder favors and, at the same time, limits the delocalization of the excitonic state. In the many-body language, this delocalized state coupled to dynamic disorder can be seen as an exciton-polaron state. Yamagata and Spano[30], for example, propose a 1D many-body hamiltonian that also introduces contributions from two and three-particle charge separated vibronic states, in addition to Frenkel-like terms. This approach results in a delocalized excitonic state that resembles a Wannier Mott exciton coupled to phonons, i. e. an exciton-polaron. These different approaches converge to a few characteristics of bandgap excitonic states that include a coherent character controlled by vibrational coupling and delocalization over many lattice sites. The short range excitonic exchange depends on the relative orientation of the HOMO (Highest Occupied Molecular Orbital) and LUMO (Lowest Unoccupied Molecular Orbital) from nearest neighbor molecules in the crystal. The formation of these one-dimensional delocalized exciton states grants H_2-OBPc the potential for efficient excitation energy transport in the coherent excitons regime.

In the work reported here, H_2-OBPc thin films with macroscopic grain size were prepared using a solution deposition technique. Incident light $\vec{K}$-vector dependent absorption experiments were performed to measure the orientation of all excitonic transition dipoles in the temperature range 4 K-300 K. Complementary

polarization-resolved photoluminescence (PL) measurements were conducted to probe the polarization of the bandgap excitons. Temperature-dependent studies indicate that delocalized excitonic states exist at low temperature (below 175 K) as a result of an interplay between short range intermolecular interactions and long-range Coulomb coupling in the presence of strong electron-phonon coupling. A total of four bandgap excitonic states evolve from the two quasi -resonant molecular Frenkel excitons, obeying Davydov selection rules. Furthermore, intermolecular interactions mix states with different symmetries and aza nitrogen orbitals, resulting in degenerate, elliptically polarized transition dipoles.

Experiment section

Thin film preparation. 1,4,8,11,15,18,22,25-octabutoxy-29H,31H-phthalocyanine (H_2-OBPc) purchased from Sigma-Aldrich was purified with recrystallization and column chromatography[31-32]. **C**-plane round-shaped single-crystal sapphire substrates were rinsed with toluene, dried with nitrogen stream and ultra-violet ozone treated for 1 h. Solution was prepared by dissolving H_2-OBPc in toluene. Spin coated (SC) thin films were prepared using a solution 2% (by weight, e.g., 2.0 mg/100 μL) at 500 RPM for 3 min. Pen-written (PW) thin films were prepared with a hollow capillary pen writing technique[33] with 0.5% solution. Thin films with macroscopic grain sizes were achieved at a writing speed of 14 $\mu m/s$. Previously reported grazing incidence x-ray diffraction experiments carried on thin films deposited under identical conditions[26-27] indicate the films are crystalline. In-situ telescope image of a H_2-OBPc PW thin film (**Figure 1**a) shows the pen-writing technique produces thin films with macroscopic grain sizes on the millimeter scale. The green spot is the quasi-monochromatic beam focused within a single grain. The image is recorded during data acquisition. An ex-situ polarized microscopic image of the same film (**Figure 1**b) shows clear color contrast between nearby grains. This is the result of different orientation of molecular stacking axes in adjacent grains where H_2-OBPc molecules are standing

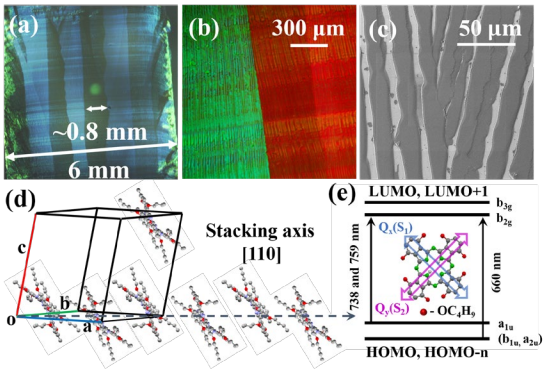

Figure 1. (a) Cross-polarized image of the quasi -monochromatic beam spot (tuned to green) incident on the H_2-OBPc thin film ,recorded in-situ, with the sample located inside the cryostat during orientation-dependent absorption experiments (b) Ex-situ cross polarized optical microscope image of two adjacent grains from the same film reveals contrast originating from different stacking axes and transition dipoles orientations (c) SEM image of the same grain boundary reveals a stripe-like configuration with molecules stacked along the axis. (d) H_2-OBPc crystal structure and molecular stacking along [110]. (e) Chemical structure or H_2-OBPc, Q-band excitons transition dipoles and energy level diagrams. The transitions from HOMO-n to LUMO are greatly enhanced in the crystalline phase.

"edge-on" the substrate to form quasi one-dimension chains (**Figure 1**d, H_2-OBPc molecular structure is shown in **Figure 1**e)[26-27, 34-35]. More images from pen-written films, deposited under different conditions along with more information about the pen-writing technique may be found in reference[27]. A Scanning Electron Microscope (SEM) image (**Figure 1**c) shows that the grains consist of straight and flat stripes oriented along the writing direction. The lack of full substrate coverage causes interference issue in absorption measurements that are addressed in supplemental information (section 3). Continuous thin films could be obtained with higher solution concentration or lower writing speed, at the cost of having overlapping grains with different crystalline axes orientation and non-uniform thin film thickness, which would introduce static disorder to the film. For this reason, we prefer to conduct the studies on the thin films with partial coverage.

Photoluminescence (PL) measurement. All PL spectra were recorded with a 2300 Princeton Instruments spectrometer coupled to a CCD camera using a 735 nm narrowband pulsed 200ps laser excitation. The laser beam was focused to a 5-micron spot on the sample mounted inside a cryostat using a microscope objective lens. The location of the excitation beam onto the sample was monitored in-situ using a long-distance telescope (**Figure 1**a). This ensured the beam was located inside the same grain as the temperature rose. The sample temperature was varied from 4 to 300 K inside a continuous-flow Oxford Microstat He cryostat. The *x*- and *y*-polarized in-plane components of the photoluminescence (I_x and I_y) were detected and the orientation (in *x*-*y* plane) of a linearly polarized exciton dipole is computed in terms of polarization, $P=(I_x - I_y)/(I_x + I_y) = \cos 2\varphi$, where φ is the in-plane rotation angle the exciton dipole moment makes with the horizontal direction.

Absorption, Linear Dichroism (LD) and Magnetic Circular Dichroism (MCD) measurements. The absorption setup schematic built with free-space optics can be found in supplemental information (section 2). Th quasi monochromatic tunable, incident light source was linearly polarized at

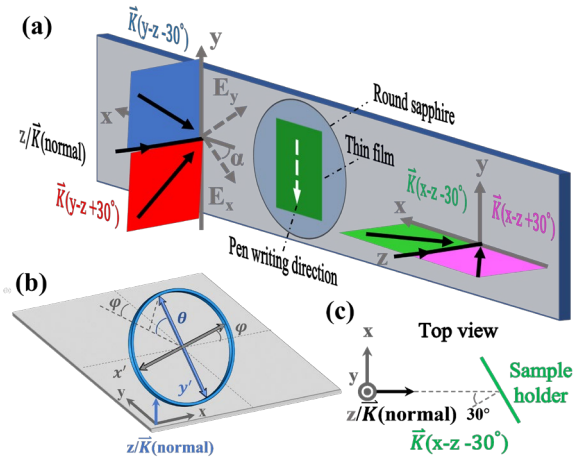

Figure 2. Schematic of incident light $\vec{K}$-vector orientations in the polarization-resolved absorption measurements. (a) Incident light $\vec{K}$ vectors orientation with respect to the (*x*,*y*,*z*) lab axes. The planes defined by the z-axis and each of the incident light $\vec{K}$-vectors orientations are highlighted with different color. At normal incidence the substrate is in the *x*-*y* plane. (b) Schematic for angular orientation of dipole frame in relation to the lab axes. θ is the rotation angle about x axis away from lab x-y plane (substrate), φ is the rotation angle about z axis within lab *x*-*y* plane. Grey vectors are contained within *x*-*y* plane, while blue vectors have out of plane components. The dipole moment coordinate system is labeled as (x', y', z'), z' is not shown for clarity. (c) Top view of the sample holder positioning in relation to the $\vec{K}$ vector of light for the case of $\vec{K}$(x-z -30°).

an angle α with respect to the horizontal direction (x-axis) (**Figure 2**a). Absorbance (A) is computed from the average of polarized light absorption spectra along orthogonal directions and is thus incident polarization independent, that is, $2A(\alpha) = 2A = A_{\parallel}(\alpha) + A_{\perp}(\alpha)$. Linear dichroism (LD) measurements were conducted by modulating the incident light polarization between orthogonal directions at 100 kHz with a photoelastic modulator PEM. LD represents the difference between angular absorbance along orthogonal directions, that is, $\mathrm{LD}(\alpha) = \mathrm{A}_{\parallel}(\alpha) - \mathrm{A}_{\perp}(\alpha)$. A lock-in technique is employed to enhance signal-to-noise and simultaneously detect the overall absorbance and the linear dichroism. Aditional experimental details can be found in reference[36]. Polarized absorbance is then calculated as $A_{\parallel}(\alpha) = \big(2A + LD(\alpha)\big)/2$ and $A_{\perp}(\alpha) = \big(2A - LD(\alpha)\big)/2$. The in-plane ($x$-$y$) orientation of a transition dipole could be estimated by finding the maximum LD(α) value recorded for its corresponding wavelength. Magnetic circular dichroism (MCD) measurements were carried out using the same setup as the linear dichroism experiments with one important modification: incident light was modulated into left and right circularly polarized at 50 kHz. Sample was mounted in a 5T Oxford superconducting magnet (MicrostatMO). Measurement was conducted at 4K. More details about MCD can be found in earlier reported research[28].

Incident light $\vec{K}$-vector dependent absorption measurement. Different incident light $\vec{K}$-vector orientations relative to the substrate were employed in order to detect the transition dipoles out-of-plane components. Four distinct $\vec{K}$-vector orientations, in addition to normal incidence, are employed as shown in **Figure 2**a. The absorption measurement for $\vec{K}$(x-z -30˚) was conducted by rotating the sample holder in the manner shown in **Figure 2**c. Other $\vec{K}$-vector orientations are realized by further rotating the sample inside the sample holder in 90˚ increments relative to the $\vec{K}$(x-z -30˚) orientation. For all absorption measurements at various $\vec{K}$-vector orientations, the incident light is focused on the sample at the same location within the thin film with the assistance of an in-situ long working distance imaging telescope.

A(α) polar plots. For each $\vec{K}$-vector orientation, average absorbance spectra and polarization-dependent linear dichroism LD(α) were measured with the incident light polarization spanning a 360° range. Spectral fit analyses were conducted to deconvolute the absorption peaks associated with distinct excitonic transitions identified in the Q-band region of the phthalocyanine molecules that spans almost the entire visible range (for a peak fit example, see supplemental information section 5). Angular absorbance values were then computed as discussed above and polarization-dependent absorbance polar plots are generated for each excitonic transition. Simulated absorbance plots were computed for comparison. Briefly, lab coordinates (xyz) were utilized to describe the measurement result ($\vec{\mu} = [\mu_x, \mu_y, \mu_z]^T$), and dipole frame (x′y′z′) was employed to characterize the nature of the transition dipole. In the present work, linear dipole ($\overrightarrow{\mu'} = [\mu_{x'}, \mu_{y'}, \mu_{z'}]^T$) and elliptical(or circular) dipole ($\overrightarrow{\mu'} = [\mu_{x'}, i \cdot \mu_{y'}, 0]^T$) were studied. In our notation, the relative orientation of the two coordinate frames could be described by θ and φ as shown in **Figure 2**b. The transition dipole components in the dipole frame $\overrightarrow{\mu'}$ were projected onto the lab coordinates $\vec{\mu}$ with the

procedure presented by Flora et al.[8] through rotation operation, $\vec{\mu} = R_z(\varphi) \cdot R_x(\theta) \cdot \overrightarrow{\mu'}$. Detailed description can be found in supplemental information (section 4). Therefore, $\vec{\mu}$ is a function of the $\overrightarrow{\mu'}$ and the dipole orientation $[\theta, \varphi]$. Simulated polar plots were then generated for a variety of $\overrightarrow{\mu'}$ and $[\theta, \varphi]$, and compared with experimental polar plots to estimate the dipole orientaion.

Results and Discussion

Excitonic transitions in individual molecules versus solid state.

Only a few experiment studies[16, 23] report on the excitonic transitions for H_2-OBPc. When compared with the parent Pc molecule[37], the absorption spectrum of H_2-OBPc molecules dispersed in toluene solution exhibits a similar splitting of the main excitonic peak (738 and 759 nm) (**Figure 3**a), associated with the band gap transitions HOMO to LUMO and HOMO to LUMO+1. The small energy difference between LUMO and LUMO+1 is due to the reduced D_{2h} symmetry of the molecule and the two pyrrole nitrogen atoms that lift the double degeneracy of the LUMO orbital. These transitions are known as Q_x and Q_y because their corresponding transition dipoles have orthogonal orientations within the Pc molecule plane[16, 26, 38]. Earlier studies also established the electrons undergo transitions between non-degenerate molecular orbitals , $a_{1u} \rightarrow b_{2g}/b_{3g}$[38]. A weak 660 nm feature also present in the absorbance spectrum is due to transitions from the HOMO-n (fourth or lower) to LUMO and may also involve aza nitrogen orbitals[23]. The polarization of these transitions is less clear as there is a controversy with regards to the possibility of

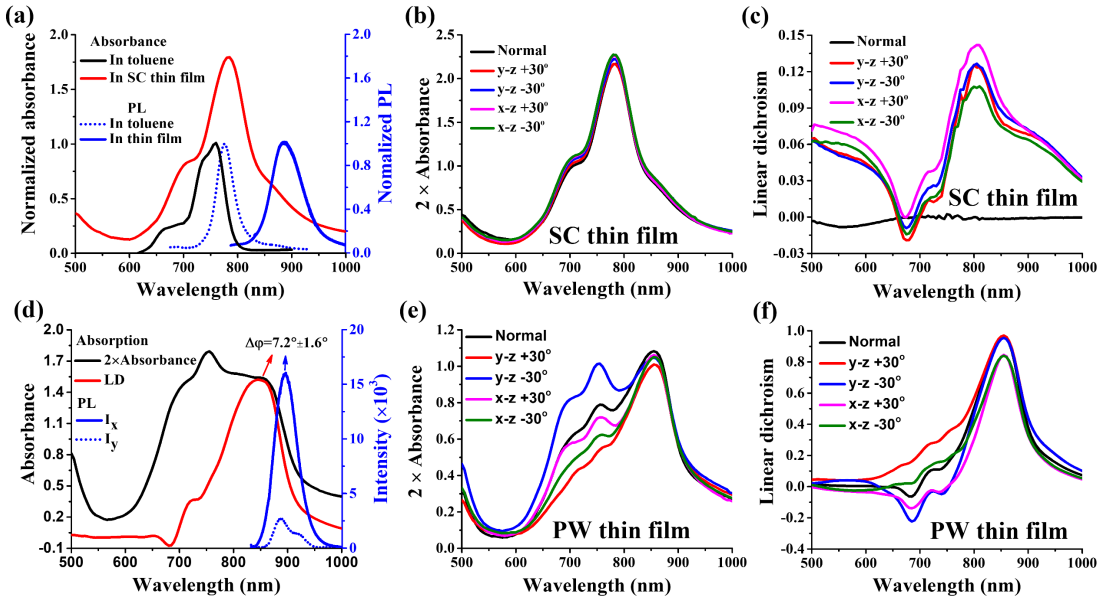

Figure 3. Absorption and PL measurements of H_2OBPc at room temperature. (a) Absorption and PL spectra of H_2-OBPc measured in toluene solution and SC thin film. (b) and (c) $\vec{K}$-vector dependent absorption and LD spectra of H_2-OBPc in the SC thin film. (d) Absorption, LD and PL spectra of H_2-OBPc in PW thin film. (e) and (f) $\vec{K}$-vector dependent absorption and LD spectra of H_2-OBPc in crystalline PW thin film.

mixing between energetically close states in the Q-band[39]. In SC thin films, the absorption spectrum is broadened and redshifted while the overall spectral shape is preserved (**Figure 3**a). The main absorption peak is now red-shifted to 785 nm. The absorbance at 685 nm is enhanced relative to the 785 nm peak, probably due to activation or enhancement of certain transitions through vibrational borrowing and lifting of the degeneracy of molecular orbitals with the onset of intermolecular interactions and disorder. More interesting, a new feature, located between 800 nm and 900 nm, is observed, indicating the possible formation of a bulk band gap exciton transition in the SC thin film. Correspondingly, PL emission peak red shifts from 780 nm for H_2-OBPc in Toluene to 890 nm in SC and PW thin films (**Figure 3**a and d). These additional transitions are much better resolved in the PW thin film (**Figure 3**d) as the absorbance spectrum clearly contains a new strong absorption feature in the 800 nm to 900 nm range which is the exclusive result of long range intermolecular interactions.

The presence of additional excitonic states can be understood in the simple framework of the Davydov model of molecular crystals[40-44], with the interplay between the distinct Frenkel exciton states S_1 and S_2 originating from the Q_x and Q_y in the free molecule (See **Figure 1**e). In H_2-OBPc crystals with two molecules per unit cell, molecules are densely packed along [110] to form a one-dimensional ordered chain (**Figure 1**d). The Davydov "oriented gas" model predicts that the molecular excitonic states S_1 and S_2 in the presence of Coulomb interactions (J_{Coul}) will each evolve into two distinct Frenkel excitonic states linearly polarized parallel (dipole -forbidden, "dark") and perpendicular (dipole-allowed, "bright") to the molecular stacking axis. We therefore expect four possible bandgap excitonic states in crystalline H_2-OBPc in the range of 800-950 nm.

As described in the introduction, recent theoretical studies[16] reveal a more complex picture of excitonic states in H_2-OBPc crystal system where strong intermolecular coupling, originating from short range exchange (J_{ex}) must be considered. Furthermore, the excitonic states become coherent at lower temperatures, a process controlled by the coupling to low energy lattice vibrations[15, 30, 45-46]. In our present work, the 855 nm transition dipole orientation in the PW thin film (measured from absorption experiments) and the 890 nm transition dipole orientation (as measured from PL experiments) differ by 7°. This confirms that the observed bandgap exciton state is the result of interactions that break the known Davydov selection rules described above[26].

Peak deconvolution of the LD and MCD spectra is performed in order to accurately identify the transitions energies and corresponding absorbances (see supplemental information section 4). Transitions centered at around 685 and 755 nm are identified, which likely involve the HOMO-n orbitals and states that originate in the aza nitrogen lone orbitals[38, 47-48]. The wavelengths associated with the four bandgap excitonic transitions born from the molecular S_1 and S_2 Frenkel excitons, are 800, 835, 865 and 920 nm.

Transition dipoles orientation in H_2-OBPc PW thin film. Incident light $\vec{K}$-vector dependent absorption spectra were measured on SC and PW thin films. The absorption spectra of SC films are almost identical regardless of $\vec{K}$-vector orientations (**Figure 3**b), lacking Linear Dichroism at $\vec{K}$(normal) (**Figure 3**c), a consequence of disorder. LD spectra at $\vec{K}$(others) ($\vec{K}$-vector orientations other than $\vec{K}$(normal)) show consistent pattern with small values compared to absorbance (**Figure 3**c), which suggests that the molecules on substrate have some preference towards forming discotic chains, as discussed in literature[7, 34]. In stark contrast, absorption and LD spectra of H_2-OBPc PW thin films (**Figure 3**e and f) are clearly distinct for different $\vec{K}$-vector orientations, indicating the transition dipoles have preferred orientations stemming from the long-range ordering in molecular stacks along the [110] crystal axis. In order to simplify the analysis, we first note that the 685 nm and 755 nm transitions have similar relative absorption strengths for different $\vec{K}$-vector orientations, which suggest that the two transition dipoles share similar orientations. Moreover, the 855 nm absorption peak and its corresponding LD contribution show similar shapes and values for different out of plane $\vec{K}$-vector orientations. This suggests that the transition dipoles around 855 nm may be linearly polarized, strictly following the Davydov splitting selection rule.

Transition dipole orientations are estimated by comparing the polarization-dependent polar absorption plots from measurement and simulation (**Figure 4**) as discussed in the experimental section. Results are summarized in **Table 1**. In the case of the 685 nm and 755 nm dipoles, their contribution to the experimental

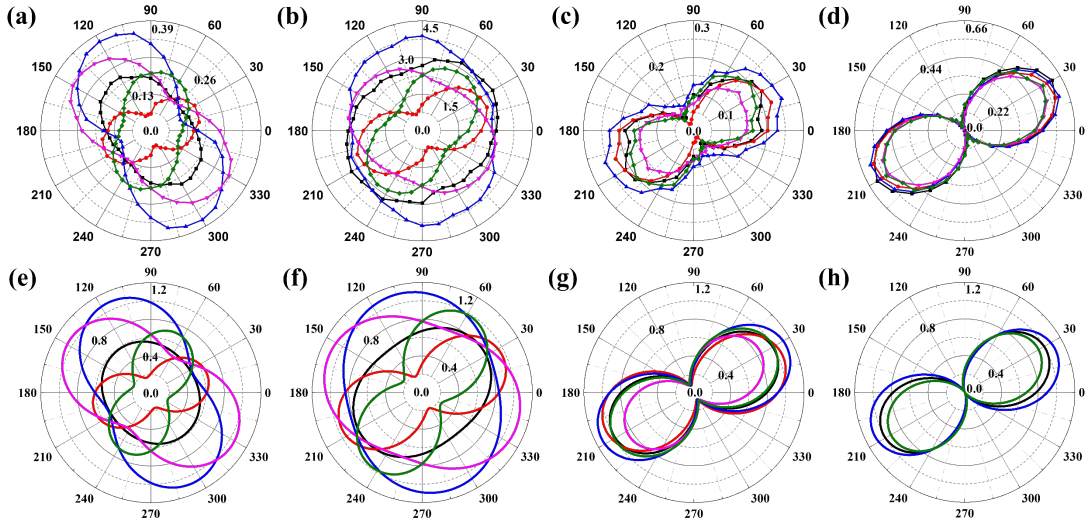

Figure 4. (a)-(d) Polarization-dependent absorbance A(α) plots at wavelengths corresponding to the four strongest transition dipoles, extracted from the k-vector dependent measurements at room temperature. (685 nm, 755 nm, 800 nm and 865 nm, respectively) The plots are color coded according to figure 1(a). (e)-(h) Simulated polarization-dependent absorbance of elliptical (685 nm), circular (755 nm) , an linear dipoles (800 nm and 865 nm, respectively. Black curves are for $\vec{K}$(normal), red for $\vec{K}$(y-z +30°), blue for $\vec{K}$(y-z -30°), pink for $\vec{K}$(x-z +30°) and green for $\vec{K}$(x-z -30°), color coded according to figure 1(a).

polarization-resolved absorption plots varies dramatically for different $\vec{K}$-vector orientations (**Figures 4**a and b). This indicates the two transition dipoles have significant out-of-plane (x-y plane) components. The 685 nm and 755 nm dipoles are indeed found to be elliptically polarized ($[0.6, i, 0]^T$ and $[0.9, i, 0]^T$, respectively) with the same long axis orientation ($[40^\circ, 28^\circ]$) relative to the lab axes. The respective simulated angular plots are shown in **Figure 4**e and f. Previous MCD studies of H_2-OBPc[23] and Pc[37] show intense magnetically activated terms in this wavelength range and suggest these transitions are circularly polarized, residing within the Pc macrocycle ring. The 755 nm dipole is almost circularly polarized, while the elliptic polarization of the 685 nm dipole may be resulted from the mixing with other non-degenerate states and phonon coupling. Previous grazing incidence X-ray diffraction study[26] conducted on these H_2-OBPc thin films indicate the [110] stacking axis is contained within the x-y plane i. e. molecules stack "edge-on" the substrate. According to the crystal geometry[25], molecules are tilted approximately 45° out-of-substrate plane along stacking axis, which is very similar to the measured out-of-plane angle of the 685 nm and 755 nm dipoles (**Table 1**). Therefore, when H_2-OBPc molecules assemble into crystalline thin films, the 685 nm and 755 nm dipoles are largely confined within a plane parallel to the molecular one.

Figure 4d shows the 865 nm and 835 nm dipoles have similar orientations at room temperature (see also Figure S6). The 865 nm dipole is linear polarized, with orientation $[0^\circ, 28^\circ]$ (**Figure** 4h for the A(α) plots from simulation). Therefore, the 835 nm and 865 nm dipoles strictly follow the Davydov excitons selection rule that state the bright (optically allowed) excitonic states are linearly polarized perpendicular to the molecular stacking axis. For the transition at 800 nm, best fitting indicate an elliptical dipole $[0.3, i, 0]^T$ with orientation $[5^\circ, -62^\circ]$ (**Figure** 4c and **Figure** 4g for the A(α) plots from experiment and simulation, repectively). This is interpreted as follows: the elliptical dipole has its major component ($\mu_{y'}$=i) tilted out of substrate plane by 5° and 28° away from *x* axis (-62° away from *y* axis), which is the direction of the 865 nm dipoles; the minor component ($\mu_{x'}$=0.3) is within substrate plane. That is, the 800 nm dipole is not fully following expected molecular selection rules. One hypothesis is that the 800 nm state is mixed with the 755 nm degenerate (circular) dipole. It should be emphasized that the absorption and MCD spectra of Pc molecules dispersed in dilute solutions or inert gas matrices (low temp exp) only report very weak signatures of transitions on the blue side of the Q_x and Q_y transitions. In conclusion, our extensive $\vec{K}$-vector dependent absorption studies indicate that the long range ordering and interactions in the pen-written crystalline thin films are responsible for: a) a new bulk (delocalized), bandgap excitonic state, characterized by a non-degenerate linearly polarized transition dipole rotated by 7° towards the [110] stacking axis and

Table 1 Summary of dipole orientations

Dipoles at RT (nm)	$\vec{\mu'}$	$[\theta, \varphi]$	Dipoles at 4 K (nm)	$\vec{\mu'}$	$[\theta, \varphi]$
685	$[0.6, i, 0]^T$	$[40^\circ, 28^\circ]$	685	$[0.7, i, 0]^T$	$[40^\circ, 28^\circ]$
755	$[0.9, i, 0]^T$	$[40^\circ, 28^\circ]$	755	$[0.9, i, 0]^T$	$[40^\circ, 28^\circ]$
800	$[0.3, i, 0]^T$	$[5^\circ, -62^\circ]$	800	$[0.3, i, 0]^T$	$[2^\circ, -62^\circ]$
835	$[1, 0, 0]^T$	$[0^\circ, 28^\circ]$	835	$[1, 0, 0]^T$	$[0^\circ, 28^\circ]$
865	$[1, 0, 0]^T$	$[0^\circ, 28^\circ]$	865	$[1, 0, 0]^T$	$[0^\circ, 28^\circ]$
			900	$[1, 0, 0]^T$	$[0^\circ, 28^\circ]$

b) a large increase in the oscillator strength and mixing of higher energy degenerate states within the Q-band. These states are particularly interesting for possible topological applications[22, 49].

Figure 5a and b show the absorption and LD spectra evolution as a function of temperature for H_2-OBPc PW thin film. The relative strength between 685 nm and 755 nm peaks is similar from 4 K to 200 K confirming the states have similar origins. When temperature drops below 175 K, the two peaks become narrower mainly due to the decrease in vibrational coupling. At low temperatures, the signature of delocalized, bulk, excitonic states is clearly present in the low temperature absorption and LD spectra at 900nm (**Figure 5a** and b). The evolution of this feature with temperature is dramatically different from the rest of the Q band spectrum, confirming the assignment to a bulk -like delocalized state, as opposed to localized Frenkel exciton. The in-plane orientations of the 855 nm and 900 nm transitions dipoles measured with LD are found to be the same and remain constant as temperature increases. Dipole orientations at 4 K were subsequently evaluated and results are show in **Table 1** (full set of polarization-resolved absorption polar plots can be found in **Figure** S7). Same out-of-plane angles were found for the 685 nm and 755 nm dipoles at room temperature and 4 K. The excitonic states 800 nm, 835 nm and 865 nm, and the additional low temperature delocalized exciton state at 900 nm are all linearly polarized within the substrate plane and pointing perpendicular to the molecular stacking axis.

Exciton-Polaron orientation in H_2-OBPc thin film. The effect of coupling to dynamic disorder on excitonic transition dipole orientation is also investigated in present work. Excitons often evolve in polaron states in small molecule crystals as a result of the strong coupling between Frenkel excitons and certain vibrational modes[15, 45, 50-51]. In this study, the formation of an exciton-polaron state is the most likely explanation for the 25 nm red-shift between the bandgap exciton identified in the absorption spectrum and the wavelength associated with the radiative recombination. **Figure 5**c shows the PL main peak intensity increases with the decreasing temperature. Similar results could be found in our previous research which involves H_2-OBPc, its "cousin"derivative H_2-$PcOC_8$[26, 52] and organic alloy compounds[27]. As discussed earlier, no obvious transition dipole rotation is observed with increasing temperature. Thus, the change of the emission peak intensity cannot be the result of a change in dipole-dipole interactions between neighboring molecules. Instead, it is likely that we are observing the formation of delocalized exciton-polarons described in the introduction. Previous studies indicate that the intermolecular interaction could enhance the exciton transport rate[16, 29, 53-54] and induce superradiant behavior[15, 45] with the formation of exciton-polarons. That is, the strong intermolecular coupling of Frenkel excitons in the presence of dynamic disorder in H_2-OBPc result in exciton delocalization across multiple molecules along the chain and the formation of a large, delocalized exciton-polaron. As a result, the PL energy could be red shifted and its intensity enhanced, especially when static disorder is absent.

In the current work, two possible delocalized exciton polaron states, characterized by wavelengths equal to 925 nm and 935 nm (marked as EX1 and EX2 from here on), are identified at low temperature (below 175 K), from the deconvolution of the PL spectra. At 4 K the two peaks have similar intensity. As temperature increases to 30 K, the EX2 intensity increases in favor of EX1. As temperature further increases to 50 K, the EX2 intensity decreases with respect to the EX1 and thus the overall PL spectrum blue shifts to 925 nm. Correspondingly, the PL peak energy (shown in **Figure 5**d) first red shifts from 1.339 eV at 4 K to 1.334 eV at 35 K, then blue shifts to 1.344 eV at 60 K. Meanwhile, the linear polarization increases from 0.607 at 10 K to 0.689 at 60 K, which indicates the radiative transition dipole rotates in x-y plane by approx. 5°. From 60 K to 150 K, the EX2 intensity further decreases in favor of the EX1 thus making the 925 nm peak dominant. Moreover, the EX1 and EX2 have similar polarization as the peak energy difference of the emission is small along orthogonal directions (I_x and I_y in **Figure 5**d). The temperature dependent polarization implies the exciton couples to lattice vibration mode and forms a delocalized polaron with different selection rules. A similar evolution of excitonic states was was previously reported for $H_2Pc\text{-}OC_8$ crystalline thin films[26]. In that system, the eight-carbon chains attached on the peripheral positions lead to less π orbital overlap. Therefore, the intermolecular interactions are expected to be weaker, and the exciton would be less affected by the lattice vibration coupling. In that case, noticeable changes in the exciton-polaron dipole orientation (as measured from polarized luminescence) were observed for temperatures as low as 75 K. Therefore, we conclude that the EX1 and EX2 observed at low temperature are coupled with lattice vibration modes and are delocalized exciton-polaron states.

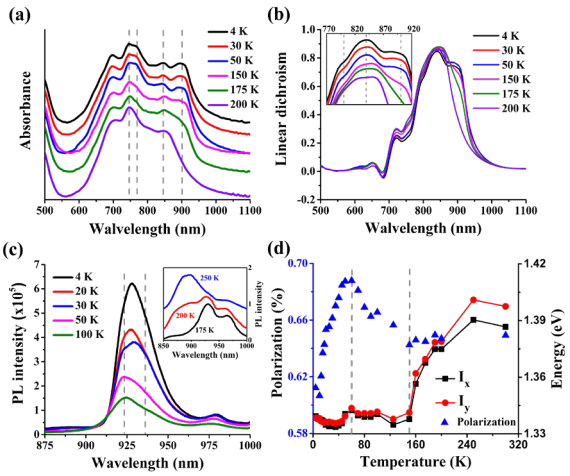

Figure 5. Temperature -dependent spectroscopy investigations of the crystalline PW film at normal incidence (a) Absorbance. (b) LD. (c) PL. (d) Linear Polarizations and energies of the main emission peaks as a function of temperature.

These states are deactivated as the emission peaks disappear when temperature exceeds 175 K, which corresponds to the dissapearance of a 900 nm peak in absorption spectra. An 890 nm emission peak starts to dominate the PL feature (**Figure 5**c insert, adapted from previous study of the Furis group[55]), leading to an overall blue shift of photoluminescence at elevated temperatures. In contrast to the EX1 and EX2, the polarization of the 890 nm PL peak remains the same from 160 K to 300 K. Previous result[26] also shows that the polarization of the 890 nm feature is temperature independent.

In conclusion the results here, corroborated with previous theoretical predictions lead to the following model for the formation of excitonic states in soluble phthalocyanine films: the bandgap excitonic states are the result of the significant short-range exchange interaction when molecules are in close contact in crystal geometry (J_{ex}), and the longer range Coulomb interactions. These excitons are identified as the 800, 835, 865 and 900 nm states, are linearly polarized within the substrate plane, perpendicular to the stacking axis. These excitons couple with intermolecular low energy phonon modes (i.e. dynamic disorder fluctuations) ($J_{ex\text{-}ph}$) to form exciton-polaron states delocalized along the stacking axis. Previous theoretical study[16] suggests the low frequency vibrations below 100 cm^{-1} and around 300 cm^{-1} control the intermolecular excitonic coupling while high energy molecular vibrations (1660 cm^{-1}) localize excitons through intramolecular vibration coupling. Our preliminary confocal Raman study on the PW thin films indicate all these vibrational modes, including the low energy phonons are clearly present in these films (see **Figure S8**). At low temperature (below 175 K), the exciton coupling with localized molecular vibrations is suppressed while the low energy phonon coupling assists the deloclaized exciton-polaron formation and results in the spreading of the wavefunction over the π-stacked molecular chain[15-16, 45, 56]. Manning et al.[27] estimate the spatial extent of the delocalized exciton along the stacking axis in H_2-OBPc system to be at least 10 lattice units. Such delocalization of the lowest-energy exciton could also be found in pentacene systems[44]. These exciton- polaron states disappear around 175 K most likely due to the onset dynamic disorder at higher temperatures. Therefore, the 890 nm Frenkel exciton state becomes the lowest energy state, that is, coupled with intramolecular vibration and localized within the molecular unit[57]. In this case, it is expected that the exciton transport would happen mainly by incoherent hopping mechanism[56]. The differences in the orientations of the transition dipoles observed in **Figure 4**d should therefore be explained as being the result of coupling with intramolecular vibration. In this model, the delocalized exciton- polaron binding energy $E_{B,del}$ could be estimated as the difference between the lowest-lying states in absorption spectrum and the PL spectrum, that is, 44.4 meV (from 900 nm to 930 nm). Similarly, the localized Frenkel-like small polaron binding energy $E_{B,loc}$ is 40.3 meV (from 865 to 890 nm). Therefore, the binding energies between the localized and delocalized polaron states are close, which suggest a possibility to tune the PL property by modifying the two couplings. For example, Manning et al.[27] successfully records the energy shift of the PL main emission peak by tuning the average H_2-OBPc molecular spacing in organic alloys, which would significantly alter the lattice vibrations. Such energy shift is mainly due to the change of the relative peak strength of the two delocalized polaron states (EX1 and EX2). By comparing the PL spectra from above study and those from current study, we could conclude that the delocalized exciton-polaron states EX2 (935 nm) are more sensitive to the dynamic disorder. Recent experiment[58] and theoretical[59] studies report that the vibration property in small organic molecules could be tuned with strain. These studies and our present results together imply a promising way to trigger the

formation of delocalized exciton polaron states at room temperature with external applied strain and enable the design of a novel semiconductor device with tunable band gap transition in the coherent excitons regime.

Conclusion

In the current study, we present an approach to directly measure the optical transition dipole orientations and characterize excitonic states in H_2-OBPc crystalline thin films using incident light $\vec{K}$-vector dependent absorption, linear dichroism and photoluminescence measurements. This approach utilizes the polarized absorption spectral evolution patterns for different incident light $\vec{K}$-vector orientations and peak fit analysis, to resolve the type (linear or elliptical) and orientation of the transition dipoles within a single crystalline grain. Orientations were measured from 4 K to room temperature. First, the larger energy transition dipoles (originating from HOMO-n states) 685 nm and 755 nm are elliptically polarized and reside in the plane of the Pc macrocycle ring. The bandgap excitonic transition dipoles (800 nm, 835 nm, 865 nm and 900 nm) are found to be linearly polarized within substrate plane and perpendicular to the molecular stacking axis. PL results show a localized exciton-polaron state with binding energy 40.3 meV and two delocalized exciton-polaron states with average binding energy of 44.4 meV. The delocalized exciton-polaron states are only present below 175 K and their transition dipole is rotated by approximately 7° towards the stacking axis. These delocalized exciton-polaron states have robust emission properties and they are potentially coherent, a highly desirable attribute in the context of developing novel semiconductor devices. Further investigations into the origins and formation/quenching mechanism of the exciton-polaron states include ultrafast pump-probe investigations and a strain-dependent photoluminescence study. The strain idea stems from the observation that the binding energies of localized and delocalized polaron states are very similar . Therefore, strain might trigger the formation of the delocalized exciton-polaron state at higher temperatures by changing low energy vibrational modes and their coupling to excitons.

Supporting Information

Schematics of thin film preparation technique; incident light $\vec{\boldsymbol{K}}$-vector orientation-dependent absorption experiment setup; treatment of raw transmitted signal in absorption measurements; generation of incident $\vec{\boldsymbol{K}}$-vector orientation-dependent absorption polar plots from experiment and simulation; peak fit analysis examples; confocal Raman spectrum measurement.

Acknowledgments

This material is based upon work supported by the National Science Foundation under Grant numbers: DMR-1056589, DMR-1919610, DMR-0821268, DMR-1828371 and the University of Vermont Sustainable Campus Fund. The authors especially thank Dr. Naveen Rawat for helpful discussions about the delocalized exciton states and UVM physics instrument shop technician Douglas Gomez for the machining of the sample holder used in low temperature $\vec{K}$-vector dependent absorption experiments.

Reference

1. Chidichimo, G.; Filippelli, L., Organic Solar Cells: Problems and Perspectives. *Int. J. Photoenergy* **2010**, *2010*, 123534.
2. Rivnay, J.; Jimison, L. H.; Northrup, J. E.; Toney, M. F.; Noriega, R.; Lu, S.; Marks, T. J.; Facchetti, A.; Salleo, A., Large Modulation of Carrier Transport by Grain-Boundary Molecular Packing and Microstructure in Organic Thin Films. *Nat. Mater.* **2009**, *8*, 952-958.
3. Diao, Y.; Tee, B. C.; Giri, G.; Xu, J.; Kim, D. H.; Becerril, H. A.; Stoltenberg, R. M.; Lee, T. H.; Xue, G.; Mannsfeld, S. C., Solution Coating of Large-Area Organic Semiconductor Thin Films with Aligned Single-Crystalline Domains. *Nat. Mater.* **2013**, *12*, 665-671.
4. Scholes, G. D.; Mirkovic, T.; Turner, D. B.; Fassioli, F.; Buchleitner, A., Solar Light Harvesting by Energy Transfer: From Ecology to Coherence. *Energy Environ. Sci.* **2012**, *5*, 9374-9393.
5. Scholes, G. D.; Fleming, G. R.; Olaya-Castro, A.; Van Grondelle, R., Lessons from Nature About Solar Light Harvesting. *Nat. Chem.* **2011**, *3*, 763-774.
6. Sze, S. M.; Li, Y.; Ng, K. K., *Physics of Semiconductor Devices*; John wiley & sons, New York, 2021.
7. Yokoyama, D., Molecular Orientation in Small-Molecule Organic Light-Emitting Diodes. *J. Mater. Chem.* **2011**, *21*, 19187-19202.
8. Flora, W. H.; Mendes, S. B.; Doherty, W. J.; Saavedra, S. S.; Armstrong, N. R., Determination of Molecular Anisotropy in Thin Films of Discotic Assemblies Using Attenuated Total Reflectance Uv− Visible Spectroscopy. *Langmuir* **2005**, *21*, 360-368.
9. Lee, J.; Roth, S.; Park, Y., Anisotropic Field Effect Mobility in Single Crystal Pentacene. *Appl. Phys. Lett.* **2006**, *88*, 252106.
10. Amaya, T.; Seki, S.; Moriuchi, T.; Nakamoto, K.; Nakata, T.; Sakane, H.; Saeki, A.; Tagawa, S.; Hirao, T., Anisotropic Electron Transport Properties in Sumanene Crystal. *J. Am. Chem. Soc.* **2009**, *131*, 408-409.
11. Uemura, T.; Nakayama, K.; Hirose, Y.; Soeda, J.; Uno, M.; Li, W.; Yamagishi, M.; Okada, Y.; Takeya, J., Band-Like Transport in Solution-Crystallized Organic Transistors. *Curr. Appl. Phys.* **2012**, *12*, S87-S91.
12. Najafov, H.; Lee, B.; Zhou, Q.; Feldman, L. C.; Podzorov, V., Observation of Long-Range Exciton Diffusion in Highly Ordered Organic Semiconductors. *Nat. Mater.* **2010**, *9*, 938-943.
13. Fraboni, B.; Fraleoni-Morgera, A.; Geerts, Y.; Morpurgo, A.; Podzorov, V., Organic Single Crystals: An Essential Step to New Physics and Higher Performances of Optoelectronic Devices. *Adv. Funct. Mater.* **2016**, *26*, 2229-2232.
14. Vagenas, N.; Podzorov, V.; Kounavis, P., Modulated-Photocurrent Spectroscopy of Single-Crystal Organic Semiconductor Rubrene with Pristine and Trap-Dominated Surfaces. *Phys. Rev. Mater.* **2021**, *5*, 063801.
15. Spano, F. C., The Spectral Signatures of Frenkel Polarons in H-and J-Aggregates. *Acc. Chem. Res.* **2010**, *43*, 429-439.
16. Fornari, R. P.; Aragó, J.; Troisi, A., Exciton Dynamics in Phthalocyanine Molecular Crystals. *J. Phys. Chem. C* **2016**, *120*, 7987-7996.

17. Nelson, T. R.; Ondarse-Alvarez, D.; Oldani, N.; Rodriguez-Hernandez, B.; Alfonso-Hernandez, L.; Galindo, J. F.; Kleiman, V. D.; Fernandez-Alberti, S.; Roitberg, A. E.; Tretiak, S., Coherent Exciton-Vibrational Dynamics and Energy Transfer in Conjugated Organics. *Nat. Commun.* **2018**, *9*, 1-9.
18. Valleau, S.; Saikin, S. K.; Yung, M.-H.; Guzik, A. A., Exciton Transport in Thin-Film Cyanine Dye J-Aggregates. *J. Chem. Phys.* **2012**, *137*, 034109.
19. Saikin, S. K.; Eisfeld, A.; Valleau, S.; Aspuru-Guzik, A., Photonics Meets Excitonics: Natural and Artificial Molecular Aggregates. *Nanophotonics* **2013**, *2*, 21-38.
20. Hou, S.; Khatoniar, M.; Ding, K.; Qu, Y.; Napolov, A.; Menon, V. M.; Forrest, S. R., Ultralong-Range Energy Transport in a Disordered Organic Semiconductor at Room Temperature Via Coherent Exciton-Polariton Propagation. *Adv. Mater.* **2020**, *32*, 2002127.
21. Brédas, J.-L.; Calbert, J. P.; da Silva Filho, D.; Cornil, J., Organic Semiconductors: A Theoretical Characterization of the Basic Parameters Governing Charge Transport. *Proc. Natl. Acad. Sci. U.S.A.* **2002**, *99*, 5804-5809.
22. Yuen-Zhou, J.; Saikin, S. K.; Yao, N. Y.; Aspuru-Guzik, A., Topologically Protected Excitons in Porphyrin Thin Films. *Nat. Mater.* **2014**, *13*, 1026-1032.
23. Kobayashi, N.; Ogata, H.; Nonaka, N.; Luk'yanets, E. A., Effect of Peripheral Substitution on the Electronic Absorption and Fluorescence Spectra of Metal-Free and Zinc Phthalocyanines. *Chem. Eur. J.* **2003**, *9*, 5123-5134.
24. Luk'yanets, E., *Electronic Spectra of Phthalocyanines and Related Compounds*. NIOPIK, Moscow, **1989**.
25. Gao, Y.; Chen, Y.; Li, R.; Bian, Y.; Li, X.; Jiang, J., Nonperipherally Octa (Butyloxy)-Substituted Phthalocyanine Derivatives with Good Crystallinity: Effects of Metal–Ligand Coordination on the Molecular Structure, Internal Structure, and Dimensions of Self-Assembled Nanostructures. *Chem. Eur. J.* **2009**, *15*, 13241-13252.
26. Rawat, N.; Pan, Z.; Manning, L. W.; Lamarche, C. J.; Cour, I.; Headrick, R. L.; Waterman, R.; Woll, A. R.; Furis, M. I., Macroscopic Molecular Ordering and Exciton Delocalization in Crystalline Phthalocyanine Thin Films. *J. Phys. Chem. Lett.* **2015**, *6*, 1834-1840.
27. Manning, L. W.; Rawat, N.; Lamarche, C.; Waterman, R.; Headrick, R. L.; Furis, M., Exciton Delocalization in H2obpc1–X Mobpc X (M= Co, Cu, Ni, Mn) Crystalline Thin-Film Organic Alloys. *J. Phys. Chem. C* **2016**, *120*, 11966-11976.
28. Rawat, N.; Pan, Z.; Lamarche, C. J.; Wetherby, A.; Waterman, R.; Tokumoto, T.; Cherian, J. G.; Headrick, R. L.; McGill, S. A.; Furis, M. I., Spin Exchange Interaction in Substituted Copper Phthalocyanine Crystalline Thin Films. *Sci. Rep.* **2015**, *5*, 1-11.
29. Chen, L.; Zhao, Y.; Tanimura, Y., Dynamics of a One-Dimensional Holstein Polaron with the Hierarchical Equations of Motion Approach. *J. Phys. Chem. Lett.* **2015**, *6*, 3110-3115.
30. Yamagata, H.; Norton, J.; Hontz, E.; Olivier, Y.; Beljonne, D.; Brédas, J.-L.; Silbey, R.; Spano, F., The Nature of Singlet Excitons in Oligoacene Molecular Crystals. *J. Chem. Phys.* **2011**, *134*, 204703.
31. Rawat, N. Exchange Mechanisms in Macroscopic Ordered Organic Magnetic Semiconductors. Ph.D. Dissertation, University of Vermont, 2015.
32. Burrill, K. Exciton Coherence in 1D Phthalocyanine Based Organic Crystalline Thin Films. Ph.D. Dissertation, the University of Vermont, 2020.
33. Wo, S.; Headrick, R. L.; Anthony, J. E., Fabrication and Characterization of Controllable Grain Boundary Arrays in Solution-Processed Small Molecule Organic Semiconductor Films. *J. Appl. Phys.* **2012**, *111*, 073716.
34. Cour, I.; Pan, Z.; Lebruin, L. T.; Case, M. A.; Furis, M.; Headrick, R. L., Selective Orientation of Discotic Films by Interface Nucleation. *Org. Electron.* **2012**, *13*, 419-424.

35. Elemans, J. A.; Van Hameren, R.; Nolte, R. J.; Rowan, A. E., Molecular Materials by Self‐Assembly of Porphyrins, Phthalocyanines, and Perylenes. *Adv. Mater.* **2006**, *18*, 1251-1266.
36. Drake, A. F., Polarisation Modulation-the Measurement of Linear and Circular Dichroism. J. Phys. E *Sci. Instrum.* **1986**, *19*, 170.
37. Hollebone, B. R.; Stillman, M. J., Assignment of Absorption and Magnetic Circular Dichroism Spectra of Solid, A Phase Metallophthalocyanines. *J. Chem. Soc., Faraday Trans. 2* **1978**, *74*, 2107-2127.
38. Fukuda, R.; Ehara, M.; Nakatsuji, H., Excited States and Electronic Spectra of Extended Tetraazaporphyrins. *J. Chem. Phys.* **2010**, *133*, 144316.
39. Mack, J.; Stillman, M. J., Transition Assignments in the Ultraviolet− Visible Absorption and Magnetic Circular Dichroism Spectra of Phthalocyanines. *Inorg. Chem.* **2001**, *40*, 812-814.
40. Basel, B. S.; Hetzer, C.; Zirzlmeier, J.; Thiel, D.; Guldi, R.; Hampel, F.; Kahnt, A.; Clark, T.; Guldi, D. M.; Tykwinski, R. R., Davydov Splitting and Singlet Fission in Excitonically Coupled Pentacene Dimers. *Chem. Sci.* **2019**, *10*, 3854-3863.
41. Davydov, A. S., The Theory of Molecular Excitons. Soviet Physics Uspekhi **1964**, 7, 145.
42. Kasha, M., Energy Transfer Mechanisms and the Molecular Exciton Model for Molecular Aggregates. *Radiat. Res.* **1963**, *20*, 55-70.
43. Lu, H.; Kobayashi, N., Optically Active Porphyrin and Phthalocyanine Systems. *Chem. Rev.* **2016**, *116*, 6184-6261.
44. Cocchi, C.; Breuer, T.; Witte, G.; Draxl, C., Polarized Absorbance and Davydov Splitting in Bulk and Thin-Film Pentacene Polymorphs. *Phys. Chem. Chem. Phys.* **2018**, *20*, 29724-29736.
45. Yamagata, H.; Spano, F. C., Strong Photophysical Similarities between Conjugated Polymers and J-Aggregates. *J. Phys. Chem. Lett.* **2014**, *5*, 622-632.
46. Ghosh, R.; Spano, F. C., Excitons and Polarons in Organic Materials. *Acc. Chem. Res.* **2020**, *53*, 2201-2211.
47. Tiedemann, M. T.; Stillman, M. J., Application of Magnetic Circular Dichroism Spectroscopy to Porphyrins, Phthalocyanines and Hemes. *J. Porphyr Phthalocyanines* **2011**, *15*, 1134-1149.
48. Ortí, E.; Crespo, R.; Piqueras, M. C.; Tomás, F., Theoretical Determination of the Molecular and Solid-State Electronic Structures of Phthalocyanine and Largely Extended Phthalocyanine Macrocycles. *J. Mater. Chem.* **1996**, *6*, 1751-1761.
49. Yuen-Zhou, J.; Saikin, S. K.; Zhu, T.; Onbasli, M. C.; Ross, C. A.; Bulovic, V.; Baldo, M. A., Plexciton Dirac Points and Topological Modes. *Nat. Commun.* **2016**, *7*, 1-7.
50. Tempelaar, R.; Stradomska, A.; Knoester, J.; Spano, F. C., Anatomy of an Exciton: Vibrational Distortion and Exciton Coherence in H-and J-Aggregates. *J. Phys. Chem. B* **2013**, *117*, 457-466.
51. Levinson, Y.; Rashba, E., Electron-Phonon and Exciton-Phonon Bound States. *Rep. Prog. Phys.* **1973**, 36, 1499.
52. Pan, Z.; Rawat, N.; Cour, I.; Manning, L.; Headrick, R.; Furis, M., Polarization-Resolved Spectroscopy Imaging of Grain Boundaries and Optical Excitations in Crystalline Organic Thin Films. *Nat. Commun.* **2015**, *6*, 1-8.
53. Aragó, J.; Troisi, A., Dynamics of the Excitonic Coupling in Organic Crystals. *Phys. Rev. Lett.* **2015**, *114*, 026402.
54. Mborong, V.; Dikandé, A., Polarons in One‐Dimensional Molecular Chains with Intermolecular and Intramolecular Vibrations. *Int. J. Quantum Chem.* **2008**, *108*, 189-197.
55. Manning, L. W. Excitonic States in Crystalline Organic Semiconductors: A Condensed Matter Approach. Ph.D. Dissertation, University of Vermont, 2016.
56. Arago, J.; Troisi, A., Regimes of Exciton Transport in Molecular Crystals in the Presence of Dynamic Disorder. *Adv. Funct. Mater.* **2016**, *26*, 2316-2325.
57. Knupfer, M., Exciton Binding Energies in Organic Semiconductors. *Appl. Phys. A* **2003**, *77*, 623-626.

58. Kubo, T.; Häusermann, R.; Tsurumi, J.; Soeda, J.; Okada, Y.; Yamashita, Y.; Akamatsu, N.; Shishido, A.; Mitsui, C.; Okamoto, T., Suppressing Molecular Vibrations in Organic Semiconductors by Inducing Strain. *Nat. Commun.* **2016**, *7*, 1-7.
59. Ruggiero, M. T.; Ciuchi, S.; Fratini, S.; D'avino, G., Electronic Structure, Electron-Phonon Coupling, and Charge Transport in Crystalline Rubrene under Mechanical Strain. *J. Phys. Chem. C* **2019**, *123*, 15897-15907.

Table of contents TOC Graphic